Numerical model for the combustion of a thermal lance

Teresa Martí-Rosselló,[†] Paul Ray,[‡] Jun Li,[†] and Leo Lue[*,†]

† *Department of Chemical and Process Engineering, University of Strathclyde, James Weir Bulding, 75 Montrose Street, Glasgow G1 1XJ, UK*

‡ *Clearwell Technology Ltd., 3 Inchloam, Durris, Banchory, Aberdeenshire AB31 6DL, UK*

E-mail: leo.lue@strath.ac.uk

Abstract

A mathematical model for the operation of a thermal lance is developed and validated, with the focus on its heat transfer and kinetics behavior. It has been found that there is a "window" of combustion rates that the thermal lance can operate, which is mainly dictated by the oxygen partial pressure. The particular value of the combustion rate can be set by adjusting the flow rate of the oxygen supply, which is practically done by manipulating the oxygen supply pressure. An open issue is the lack of experimental kinetics data for thermal lance combustion.

1 Introduction

A thermal lance consists of a hollow metallic tube, generally made of iron or steel, which can also be filled with metallic wires. It is generally used to cut metals or other materials, like concrete.[1] The basic working mechanism consists of injecting pure oxygen from one end with an ignition source at the opposite end of the lance. When the ignition temperature is

reached, combustion occurs, and the lance will self-consume, generating heat and iron oxides in the process. The resulting heat is able to cut other materials by either melting them, such as in the case of iron, steel or other metals, or by burning them, thereby releasing more heat.

A simplified, schematic drawing of the combustion of an iron rod is shown in Fig. 1. The rod is divided into three main zones: solid iron, a layer of molten iron, and a layer of liquid iron oxide. Combustion occurs within the molten iron oxide zone at the far left of the diagram. Although the molten iron oxide and molten iron layers are separated by a distinct boundary in the diagram, in actuality, the composition within the molten iron oxide layer will vary continuously from very little iron at the far left boundary to pure iron at the right boundary with the molten iron layer. There is no well defined boundary between the molten iron oxide and molten iron layers. Oxygen absorbs within the iron oxide zone, and more of the combustion occurs towards the right of the zone. The molten iron oxide attached to the solid iron will continuously detach from the rod, such as by gravity or, as typical in the case of a thermal lance, swept away with the oxygen flow. As the rod self-consumes, the reaction zone moves to the right. The combustion of iron consists of four main steps, which repeat in a cycle: iron melting, oxygen absorption into the molten phase, reaction of the absorbed oxygen with the molten iron generating heat and iron oxide, and detachment of molten material from the solid iron. The steps take place simultaneously, but they are a cause/reaction of each other in a self-sustained combustion process, provided that the initial heat required to reach the ignition temperature is supplied.

The intrinsic reaction kinetics of iron combustion are not fully understood. The determination of the chemical kinetics was attempted by Wilson et al.[2] based on experimental measurements of the combustion of an iron rod in a stationary, pressurized oxygen atmosphere. This type of experiment provides deep insight in the process of iron combustion, but it cannot completely explain the combustion behavior of a thermal lance, because it disregards the influence of the oxygen flow, which continuously removes the molten material from the burning tip. The rate law suggested by Wilson and co-workers[2] describes the

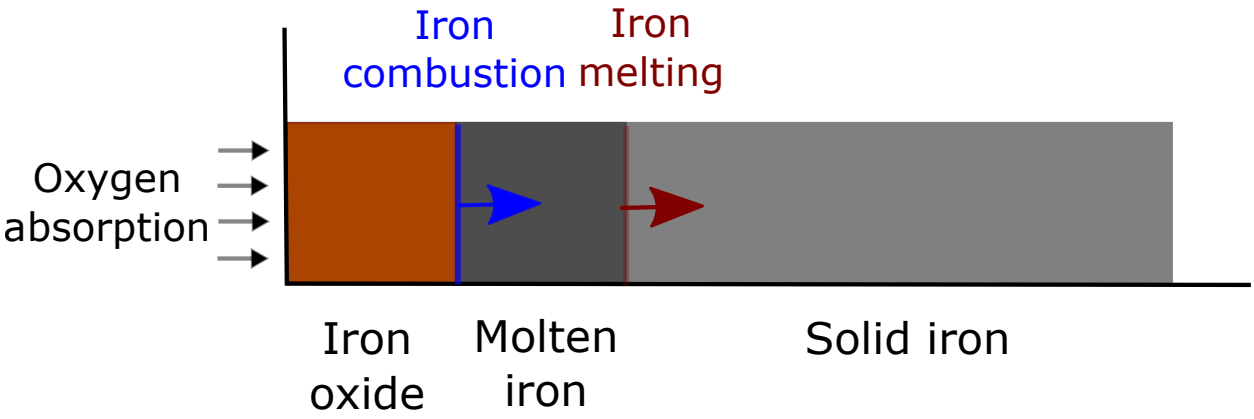

Figure 1: Schematic diagram of the combustion of an iron rod.

kinetics with the Arrhenius equation and a dependence on the oxygen partial pressure and the oxygen absorption equilibrium constant. A simplified version has been validated for low oxygen partial pressures,[2] which would make it suitable for a thermal lance operating at atmospheric pressure.

Commercial thermal lances usually include a basic set of instructions on their operation. Some of them are summarized in Section 3, but there is not much peer-reviewed work published on the operation of a thermal lance. The usual approach on how to operate a thermal lance is by performing experimental trials that give enough information about how to operate it, but without analyzing the process in detail. Some attempts have been made to understanding the underlying physical and chemical mechanisms of thermal lances, both experimentally and through modeling. Models for the operation of thermal lances are not abundant in the literature. Shabunja et al.[3] presented a mathematical model describing the combustion and melting of an iron rod in a stagnant oxygen atmosphere. They calculate the melting velocity with an expression that accounts for a difference in temperature between the melt and the drop. They also determined, by fitting, a velocity for the oxygen transport into the drop, and they recommend to include the modelling of the oxygen absorption with a pressure dependence. The work of Lynn et al.[4] present a time-dependent model for the combustion of metal rods, where the temperature profile and the regression rate of the

melting interface are studied .

Wang et al.[5] developed a thermal lance model that includes the iron combustion kinetics determined by Wilson et al.[2] The model described the temperature profile along the thermal lance, but the temperature used to determine the rate of reaction was not consistent with the predicted temperature profile.

The main gap, apart from the lack of abundant literature on the topic, is to find the intrinsic kinetics of iron combustion, and to be able to predict the thermal lance behavior in relation to the iron combustion kinetics. The aim of this work is to understand better the processes involved in the combustion of a thermal lance as a whole. There is literature on the kinetics of iron combustion, and there are a few models that predict how a thermal lance is consumed, but this is the first model that attempts to make the combustion kinetics of iron and the thermal lance model consistent with each other.

The remainder of this paper is structured as follows. Section 2 reviews the previous experimental studies on kinetics of iron combustion. A parameterized rate law expression for the combustion kinetics, which is used in the work, is also presented. Section 3 explains the operation of a thermal lance, including how the pressure of the oxygen injected to the thermal lance translates into different oxygen velocities. Section 4 describes the mathematical model of a thermal lance being consumed due to combustion. In Section 5, the model of iron combustion is combined with the model of a thermal lance to find a consistent rate of combustion for the thermal lance, and finally Section 6 summarizes the main findings.

2 Oxidation kinetics of iron

The combustion kinetics of a thermal lance correspond to the oxidation kinetics of its constituent materials, which generally consists of iron or steel. This section reviews the literature on the kinetics of iron combustion, from the experiments performed to study it to the suggested rate laws and kinetic parameters.

Steinberg and co-workers performed combustion experiments on vertical rods of iron in a stagnant oxygen atmosphere.[6–8] The bottom end of the rod was ignited, and they observed that a molten oxide droplet forms at the ignition end of the rod, which grows until it detaches from the rod due to gravity. When this droplet falls to the bottom of the combustion chamber, bubbles of gas are observed to form and burst from the molten oxide droplet as it cools. These bubbles are thought to be excess oxygen in the molten material remaining after the iron had already fully oxidized. From these observations, Steinberg et al. concluded that the combustion of iron takes place in the liquid phase, and that its limiting mechanism is not the oxygen absorption to the molten iron, but the combustion reaction itself, at least for the rod diameter of 32 mm and the oxygen pressure in the chamber of 6.9 MPa.

However, Shabunja et al.[3] observed that for experiments of combustion of iron rods of diameters between 2 and 7 mm and for atmospheric oxygen pressure, despite most of the molten material consisted mainly of iron oxides, it could also contain molten iron that did not have time to react completely before being detached. They concluded that the molten material can detach from the solid rod before it has time to completely oxidise, and that when the molten material remains attached to the lance tip for a longer time, the tip temperature increases because a higher extent of oxidation of the molten iron into iron oxide can be achieved.[3]

Wilson et al.[2] analyzed experimental data[9,10] of combustion of iron rods also in an enclosed, oxygen-filled chamber at pressures varying between 3 and 100 bar. Figure 2 shows their results. They observed that the rate of reaction increases with temperature, as expected, but it also depends on the diameter of the rod. Although the mass rate of iron consumption increases for larger diameters, the velocity of consumption decreases. The burning velocities reported in Wilson et al.[2] range from 0.2 to 1.6 $\mathrm{cm\,s^{-1}}$ for different rod diameters and oxygen pressures in the chamber, similar velocities between 0.4 and 1.4 $\mathrm{cm\,s^{-1}}$ for diameters between 0.7 and 0.2 cm and 70 bar of oxygen pressure in the chamber are also

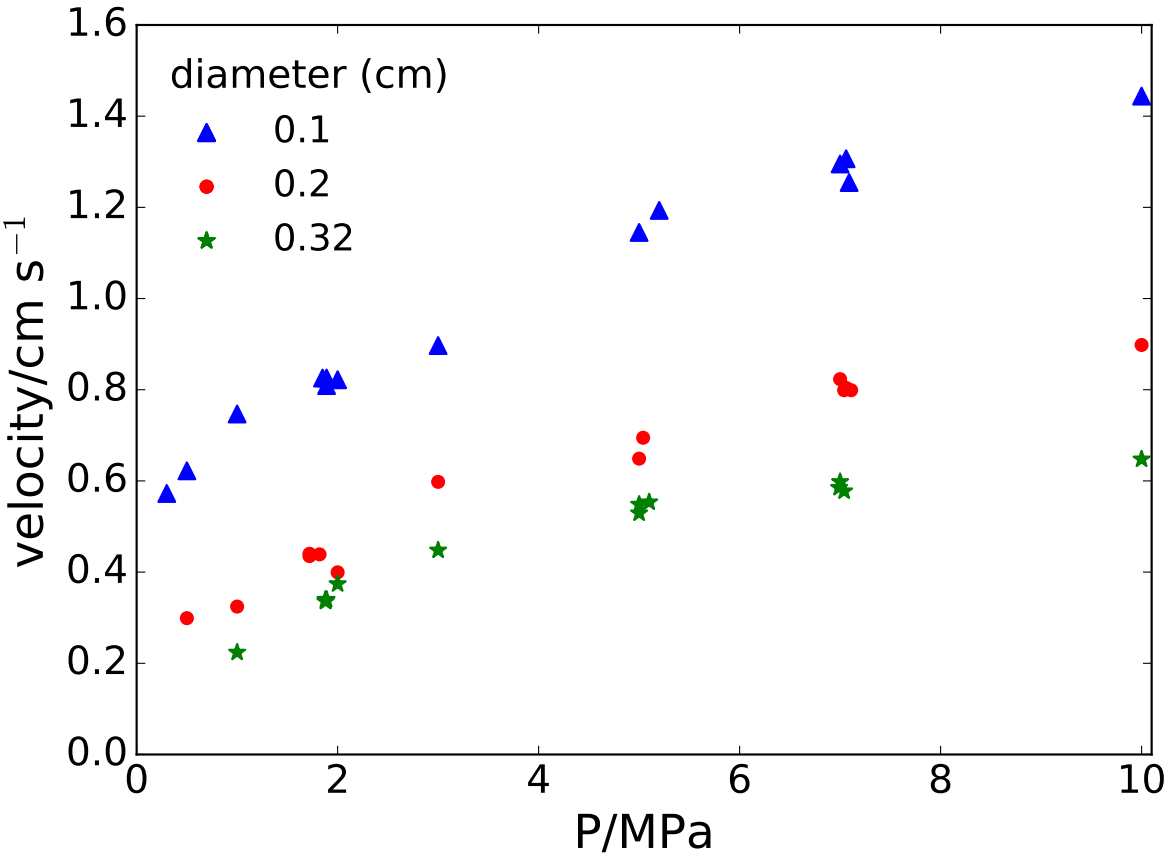

Figure 2: Combustion velocity of iron rods of different diameters in a stagnant oxygen atmosphere. The data are from Ref. 2.

reported in the literature (see Ref. 11 as in Ref. 3).

Suvorovs[11] explains the decreasing combustion velocity for larger rod diameters with a drop detachment and heat transfer theory. The diameter of a rod is related to the cross-sectional area, therefore a larger diameter implies a larger cross-sectional area, which will produce larger amounts of molten material that at some point will be detached from the rod due to gravity. Smaller molten drops will detach less frequently than larger drops because they are less heavy, allowing more time for the heat to transfer from the molten material to the solid rod. This would explain why larger rod diameters have slower burning rates than smaller diameters. The rate at which the volume of molten material attached to the rod

increases for larger diameters does not increase linearly. When the surface area increases, the increase in molten material slows down. The burning rate decreases with increasing rod diameter up to the point where, unless the oxygen pressure in the chamber also increases, the self-sustained combustion will stop.

With respect to the impact of the elevated oxygen pressure on the rate of reaction, Wilson et al.[2] suggested that the rate of combustion should not increase indefinitely with pressure; at a given pressure it should reach a plateau and the combustion velocity should become independent of the oxygen pressure. The pressure of oxygen is related to the oxygen availability to react with the molten iron, but when there is already enough oxygen to react with all the molten iron, a further increase of the oxygen pressure should not make a difference. They suggested that the combustion process follows the Langmuir-Hinshelwood-Hougen-Watson (LHHW) mechanism,[2] which takes into account the adsorption/desorption of reactants on the surface and is widely used for fluid-solid reactions. For the combustion of iron rods, the reaction rate per cross-sectional area of the rod, denoted by R_{Fe}, takes the form[2]

$$R_{\mathrm{Fe}} = \frac{k(T)K(T)P_{\mathrm{O_2}}^{1/2}}{1 + K(T)P_{\mathrm{O_2}}^{1/2}}, \tag{1}$$

where $k(T)$ is the Arrhenius rate constant determined for the temperature of the molten iron at the tip of the lance, $P_{\mathrm{O_2}}$ is the oxygen partial pressure, and $K(T)$ is the equilibrium constant for oxygen adsorption by molten iron oxide. The parameter $K(T)$ is temperature dependent and controls the amount of oxygen available to react with the molten iron, and it might be related to the rod diameter of the molten droplet. The oxygen pressure that appears in the rate of reaction corresponds to the chamber pressure in the case of a chamber filled with oxygen, but it corresponds to atmospheric pressure in the case of a thermal lance burning in atmospheric conditions. This oxygen pressure should not be mistaken by the pressure of injection of the oxygen.

At low oxygen pressures, where $KP_{O_2}^{1/2} \ll 1$, the reaction rate is approximately proportional to $P_{O_2}^{1/2}$, but at high oxygen pressures where $KP_{O_2}^{1/2} \gg 1$, the molten iron oxide droplet becomes saturated with oxygen, and, consequently, the reaction rate no longer depends on the pressure of oxygen.

The kinetic parameters of the rate constant can be adjusted for a given oxygen pressure. The kinetic parameters are the pre-exponential factor A and the activation energy E. The rate constant is given by the Arrhenius expression

$$k(T) = A \exp\left(-\frac{E}{RT}\right) \tag{2}$$

where R is the gas constant, and T is the temperature of the molten iron that reacts with oxygen.

Theoretically, the oxygen is physically and chemically adsorbed according to equilibrium constants that depend on the oxygen pressure, temperature, the number of adsorption sites per unit area, and the concentration of oxygen,[12] but so far no numerical values have been used in the literature to describe the oxygen adsorption/absorption in molten iron and in molten iron oxide. Given that the oxygen equilibrium constant is unknown, a simplification of the rate law that lumps the adsorption constant with the Arrhenius rate constant has been validated for oxygen pressures between 0.3 and 10 MPa and rod diameters between 10 and 20 mm, and for oxygen pressures between 0.3 and 5 MPa and a rod diameter of 32 mm

$$R_{Fe} \simeq k'(T) P_{O_2}^{1/2}, \tag{3}$$

where the parameter $k'(T)$ incorporates the effect of oxygen adsorption. As already mentioned, this expression is not suitable for high oxygen pressures, because it has been observed that the rate of reaction does not keep indefinitely increasing with increasing pressure.[2]

The value of the activation energy determined by Wilson et al.[2] is $E = 246.8\,\mathrm{kJ\,mol^{-1}}$, and different values of pre-exponential factors are given depending on the rod diameters of

0.1, 0.2, and 0.32 cm, but their apparent pre-exponential factor also includes other parameters depending on the form of the rate of reaction .[2]

In this work, given that the rate of reaction including the Arrhenius expression is of the form

$$R_{\mathrm{Fe}} = \frac{A \exp\left(-\frac{E}{RT}\right) K P_{\mathrm{O_2}}^{1/2}}{1 + K P_{\mathrm{O_2}}^{1/2}}, \tag{4}$$

a parameter $A' = AKP_{\mathrm{O_2}}^{1/2}$ will be used to combine all the unknown factors in the previous expression, resulting in the following combustion rate

$$R_{\mathrm{Fe}} = A' \exp\left(-\frac{E}{RT}\right). \tag{5}$$

Under normal operating conditions, the oxygen partial pressure at the lance tip will be nearly atmospheric (in the case of using pure oxygen).

3 Operation of a thermal lance

The operative principles of a thermal lance are reviewed in this section. For a thermal lance to start burning it requires to be heated at one end while at the same time oxygen is introduced from the opposite end, and combustion occurs when the oxygen reaches the hot end of the lance. A thermal lance consists of an iron tube filled with iron rods/wires, Fig. 3 shows how the iron rods run inside the thermal lance, but there is still some remaining space between the rods for oxygen to flow.

The critical parameters that determine if combustion occurs are the oxygen partial pressure and the temperature of the tip of the lance. If the temperature is not sufficiently high or if there is not enough oxygen in contact with the hot end of the lance, combustion will not take place.

According to Wilson et al.,[2] the minimum ignition temperature of an iron rod is 1600 K,

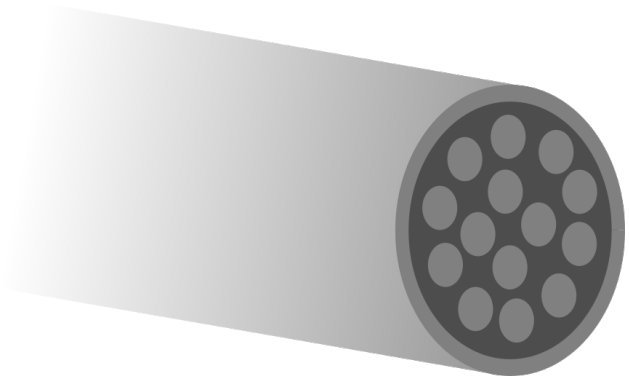

Figure 3: Diagram of a thermal lance with inner rods.

and so it is expected that the tip temperature should be equal or higher than 1600 K. The adiabatic flame temperature gives an upper bound to the tip temperature. This value depends on the particular conditions of the combustion: In the literature, a variety of estimated adiabatic temperatures can be found: 2250 K[13] (in air at constant pressure), 2490 K[14] (in air at constant volume), and 3400 K[2,15] (in pure oxygen at constant pressure).

One way to experimentally determine the temperature of the iron during combustion is from the droplets of molten material. Shabunja et al.[3] estimated the temperature of the droplets of molten material to be about 2200–2800 K, which is lower than the temperature of 3600 K determined by Steinberg et al.[7] in experiments with reduced gravity, where the droplets do not separate from the iron rod. It is argued that when the droplets separate from the rod, they do not have time to completely oxidize to generate more heat.

The backpressure required for a thermal lance at atmospheric conditions has to be at least slightly higher than the atmospheric pressure. An analysis in more detail of the oxygen delivery pressure is given in Subsection 3.1.

A summary of the operating conditions reported in some instruction manuals from commercial thermal lances[16–20] can be found in Table 1. The recommended operating back pressures of oxygen are between 1 and 17 bar. The maximum oxygen back pressure corresponds to a value of the oxygen flow rate at which the combustion process extinguishes due to the high loss of heat from the combustion zone to the oxygen flow.

Table 1: Thermal lance diameter D, length L, operating oxygen pressure P_{O_2}, and estimated reaction temperature T obtained from the instruction manuals of commercial thermal lances.

Source	D / mm	L /m	P_{O_2} / bar	T / K
Minco Pipe[16]	3-50	0.3–0.5	7–17	1922–6822
Tube Special[17]	10–20	—	5.5–7	—
Daiwa Lance Int.[18]	13–27	2.75–3	8–12	> 3273
Humberg[19]	12.5–21	1.5-6	6–8	2473
Broco Prime-cut[20]	5–13	—	1–5.5	5811

The velocity of combustion of a thermal lance has not been reported in many studies. Wang et al.[5] reported an experimental velocity of combustion of $0.77\,\mathrm{cm\,s^{-1}}$ for a thermal lance at atmospheric conditions, although no specifics on the thermal lance dimensions used in the experiment are mentioned. In the same work, a tip temperature above 2000 K is measured, which they say is not reliable because the flame was flickering and the temperature of the flame surface is much lower than the inside flame temperature, so the expected temperature would be higher than that. Another similar experiment[21] with a thermal lance of the dimensions reported in Section 4 yielded a combustion velocity of $0.8\,\mathrm{cm\,s^{-1}}$, similar to the one reported by Wang et al.[5]

It is not obvious whether a thermal lance burning with continuous oxygen flow will self-consume more quickly or more slowly than an iron bar in a stagnant oxygen environment. In a system with flowing oxygen, the molten material will not remain attached to the solid iron for long, and that might decrease the temperature of the tip in comparison with a bar in a stagnant oxygen. If the temperature of the tip decreases, the rate of reaction will decrease. Another factor that acts to decrease the tip temperature is the heat lost to the oxygen flow by thermal convection. On the other hand, at low oxygen pressures the melting velocity depends on the extent of reaction,[11] and if oxygen is constantly blowing without the layer of oxide acting as a barrier, the extent of reaction will always be 100% and the velocity of iron consumption and melting might actually increase.

3.1 Delivery of oxygen

In this section, the required backpressure of oxygen is discussed. The equations that describe the pressure drop along a pipe are used to know how the oxygen backpressure translates in terms of oxygen velocity, to use it later in the energy balances in Section 4. The pressure drop along the lance has been calculated for fluid in a pipe with the following expression

$$\frac{dp}{dy} = -\frac{2\rho_{O_2}(p)v_{\mathrm{O_2}}^2(p)}{D_H} f(p) \tag{6}$$

where y is distance from the lance entrance, ρ_{O_2} is oxygen density that might change with pressure p, and f is the friction factor. For turbulent flow in a pipe at high Reynolds number (i.e. $\mathrm{Re} \geq 4000$), the friction factor can be estimated by[22]

$$f = 0.079\mathrm{Re}^{-1/4} \tag{7}$$

$$\mathrm{Re} = \frac{D_H v_{\mathrm{O_2}} \rho_{\mathrm{O_2}}}{\mu_{\mathrm{O_2}}} \tag{8}$$

where D_H is the diameter of the pipe, $v_{\mathrm{O_2}}$ is the velocity of the oxygen, and μ is its dynamic viscosity. For pipes with complex geometrical cross-sections, the hydraulic diameter is used, which is defined as $D_H = 4A/P_{wet}$, where A is the flow area of the inner cross-section and P is the wetted perimeter of the cross-section. The velocity is calculated according to

$$v_{\mathrm{O_2}} = \frac{\dot{m}_{\mathrm{O_2}}}{\rho_{\mathrm{O_2}} A}, \tag{9}$$

where $\dot{m}$ is mass flow rate.

Figure 4 shows how different oxygen back pressures translate into different oxygen mass flow rates depending on the length of the lance. The maximum oxygen back pressure should be determined with the energy balance of the thermal lance (see Section 4), and the minimum pressure should be above the corresponding atmospheric pressure. The minimum oxygen back pressure is the one that allows the minimum oxygen mass flow required for steady-state

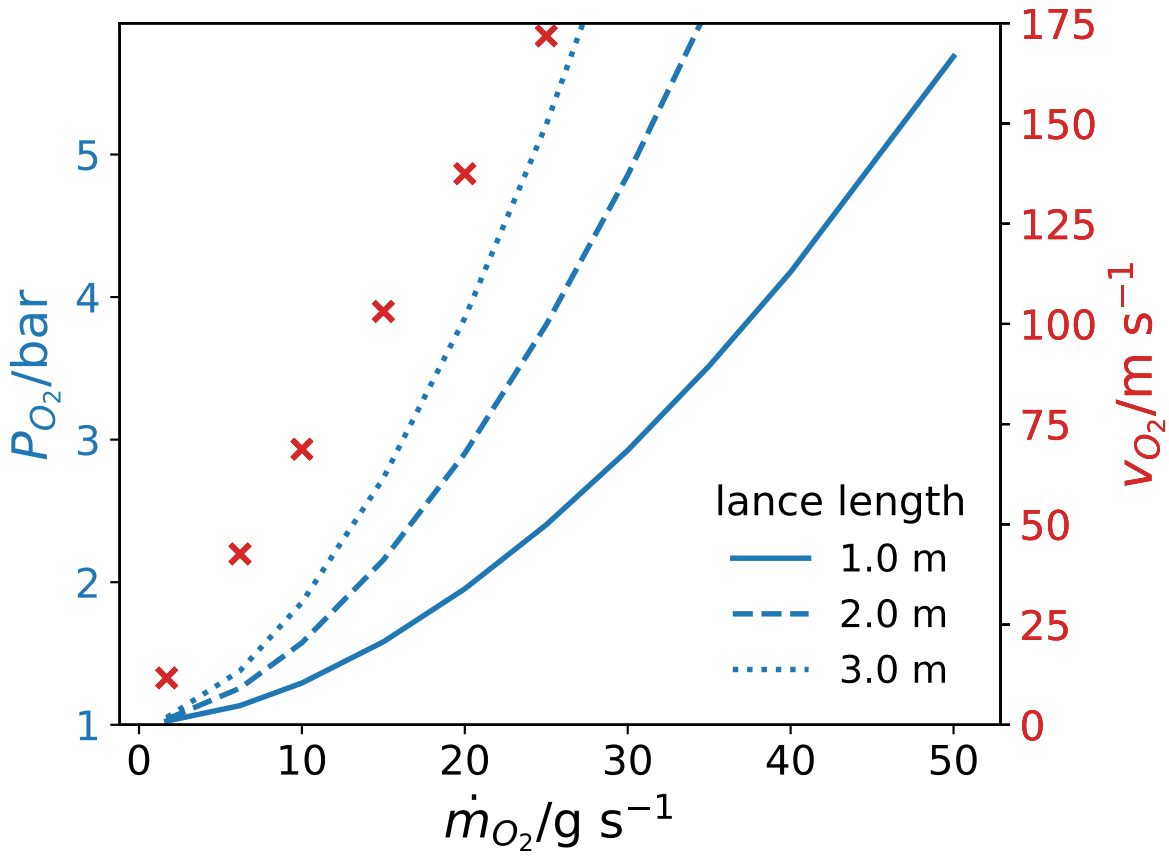

Figure 4: Dependence of oxygen mass flow rate on the oxygen back pressure for a lance length of 1 m (solid line), 2 m (dashed line), and 3 m (dotted line); and dependence of the oxygen velocity inside the lance, on the oxygen mass flow rate (crosses).

rate of combustion. In this case, for the given lance dimensions (see Table 2), the minimum oxygen mass flow rate required is $1.7\,\mathrm{g\,s^{-1}}$.

4 Thermal lance model

In this work, the thermal lance consists of an iron tube filled with iron rods (see Fig. 3), and the diameter of the lance and the rods are given in Table 2. A one-dimensional model is used to study the operation of a thermal lance at steady-state. Variations in temperature and other properties are assumed to occur only along the longitudinal axis of the lance; changes

along the radial directions are neglected.

The thermal lance is divided into three main layers, pictured in Fig. 1: solid iron, molten iron, and iron oxide. The longest layer is the solid iron layer, which is in contact with a molten iron layer. The interface between these two layers continuously recedes as the solid melts from the heat generated by the combustion of the lance tip. The end of the molten iron layer is continuously consumed by the combustion reaction to form iron oxide at the end of the thermal lance. The iron oxide layer is assumed to be thin and have a uniform temperature that is equal to the temperature of the end of the molten iron layer. Oxygen absorbs into the this layer. The oxygen flow detaches iron oxide from the lance tip at the same rate as it is generated by the oxidation reaction.

The combustion rate is assumed to only depend on the temperature of the oxide layer (i.e. the tip temperature of the lance) and on the oxygen partial pressure, in this case atmospheric pressure. The tip temperature used in the calculation of the rate of combustion at that end of the lance needs to match the temperature predicted by the energy balance, therefore, the solution of the model will be found where both models agree. The influence of the interface between solid and liquid iron is analytically studied to have an idea of how it can affect the temperature distribution of the thermal lance, but it has been excluded from the full model for simplification purposes, since the ignition temperature of iron of 1588 K at a 1 atm oxygen pressure[23] is below its melting temperature 1811 K. As long as sufficient oxygen is available, it is expected that the iron will react as soon as it melts. The ignition temperature versus the oxygen pressure was studied by Bolobov et al.,[24] they performed combustion experiments with iron and steel rods of 1.5 and 3 mm and at oxygen pressures between 0.2 and 50 MPa, and they concluded that, at least for their experimental range of pressures, the ignition temperature did not have a strong dependence on the oxygen pressure. The ignition temperatures were measured by a contact method, and they were between 1523 and 1613 K.

The combustion of iron generates iron oxide as a product with different levels of oxidation, the three stable oxide compounds are FeO, Fe_2O_3 and Fe_3O_4. The oxidation level of the

product depends on the temperature and the excess of oxygen available, but above 2000 K only FeO is found in the product.[6] If there is excess of oxygen that has been dissolved in the liquid iron and liquid oxide, the remaining iron oxide can be generated during the cooling of the molten product, additionally, remaining dissolved oxygen can be released in the form of gas during the cooling period if the product has already reached the maximum oxidation level. In this work, only the reaction $Fe + \frac{1}{2}O_2 \rightarrow FeO$ is included, because this model is only focused on the heating and combustion of the thermal lance.

The combustion of iron also generates heat, some of which is used to melt the solid iron and raise its temperature, and some is lost to either the inner oxygen flow or to the surrounding air.

The mathematical model used in the current work is based on the one-dimensional stationary model from Wang et al.,[5] but instead of using the combustion kinetics from Wilson et al.[2] without modification, the kinetics have been adjusted in order to make the temperature used in the kinetics calculation consistent with the energy balance of iron, and also to obtain a rate of reaction consistent with available experimental data from the combustion of thermal lances.

4.1 Model parameters

The thermal lance is modeled as a bundle of n iron rods, each with diameter d_r, that are encased in an iron tube with inner diameter d_i and outer diameter d_o. These dimensions and the other parameters used in the model are summarized in Table 2. Oxygen and air are assumed to behave as ideal gases, and their properties are fixed at their values at a temperature of 25°C and a pressure of 1 atm. The values referring to iron have been determined with correlations depending on the temperature, which are explained in this section.

The main thermo-physical properties of iron, oxygen and air are also given in this table, such as the thermal conductivity (λ_{Fe}, λ_{O_2} and λ_a), the density (ρ_{Fe}, ρ_{O_2} and ρ_a), and the heat capacity ($C_{p,Fe}$, C_{p,O_2} and $C_{p,a}$). The iron density used in the model (ρ_{Fe}) is given by the

Table 2: Values of the parameters used in the model.

parameter	value	notes
d_o (cm)	1.6	
d_i (cm)	1.4	
d_r (cm)	0.2	
n	14	
T_a (°C)	25	is the same as T_∞
σ ($\mathrm{W\,m^{-2}\,K^{-4}}$)	5.67×10^{-8}	
ϵ_{Fe}	1	
ϵ_{FeO}	1	
$\rho_{\mathrm{Fe,s}}$ ($\mathrm{kg\,m^{-3}}$)	7874	
ρ_{Fe} ($\mathrm{kg\,m^{-3}}$)	correlation	Eq. (10)
$\rho_{\mathrm{O_2}}$ ($\mathrm{kg\,m^{-3}}$)	1.291	at 25°C and 1 atm
ρ_a ($\mathrm{kg\,m^{-3}}$)	1.225	at 25°C and 1 atm
$C_{p,\mathrm{Fe}}$ ($\mathrm{J\,kg^{-1}\,K^{-1}}$)	824.3	constant after 2000 K
$C_{p,\mathrm{FeO}}$ ($\mathrm{J\,kg^{-1}\,K^{-1}}$)	949.7	constant after 1600 K [25]
$C_{p,\mathrm{O_2}}$ ($\mathrm{J\,kg^{-1}\,K^{-1}}$)	920	at 25°C and 1 atm
$C_{p,a}$ ($\mathrm{J\,kg^{-1}\,K^{-1}}$)	1006	at 25°C and 1 atm
λ_{Fe} ($\mathrm{W\,m^{-1}\,K^{-1}}$)	correlation	Eq. (11)
$\lambda_{\mathrm{O_2}}$ ($\mathrm{W\ m^{-1}\ K^{-1}}$)	0.026	at 25°C and 1 atm
λ_a ($\mathrm{W\,m^{-1}\ K^{-1}}$)	0.026	at 25°C and 1 atm
ΔH_c ($\mathrm{kJ\,kg^{-1}}$)	−4537.6	from Ref. 25
$\mu_{\mathrm{O_2}}$ (Pa s)	2.055×10^{-5}	at 25°C and 1 atm
μ_a (Pa s)	1.18×10^{-5}	at 25°C and 1 atm

correlation in Eq. (10). However, a constant density of solid iron ($\rho_{\mathrm{Fe,s}}$) is used to determine the minimum oxygen required for the combustion of the given mass of iron. Properties related to the iron oxide were also required in the boundary conditions: λ_{FeO} and $C_{p,\mathrm{FeO}}$. Some properties are specific to the solid, like the emissivity constant for iron ϵ_{Fe} and iron oxide ϵ_{oxide}, others are specific to the fluids, like the oxygen viscosity $\mu_{\mathrm{O_2}}$ and the air viscosity μ_a. The heat released from the combustion of iron ΔH_c is estimated for $\mathrm{Fe} + \frac{1}{2}\mathrm{O_2} \rightarrow \mathrm{FeO}$ using the enthalpies of formation at 3000 K, and the surrounding temperature T_∞ is the temperature of the air T_a, which corresponds to the initial temperature of the lance.

Based on two density correlations for liquid iron, one for a temperature range between 1809 and 2480 K [26] and another for a temperature range between 1900 and 5000 K, [27] and for solid iron in the temperature ranges 673–1183 K, 1183–1673 K and 167–1812 K, [28] a single expression approximating the ρ_{Fe} in $\mathrm{kg\,m^{-3}}$) across temperatures from the liquid to solids

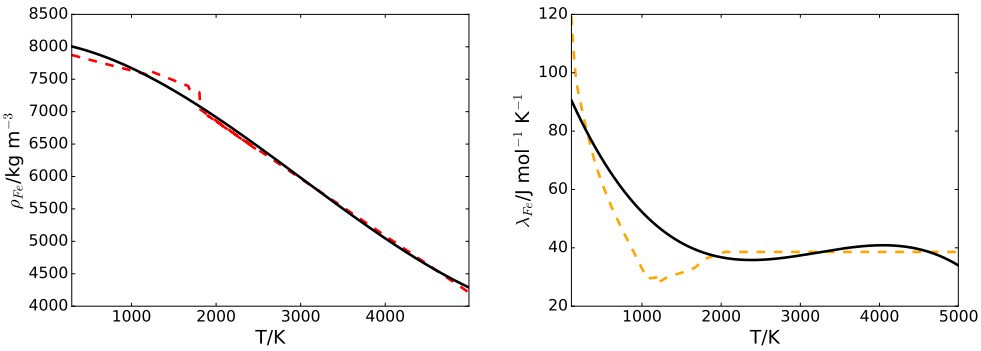

(a) Density of iron.

(b) Thermal conductivity of iron.

Figure 5: Density and thermal conductivity correlations fitted as a single curve (solid line) to the literature values (dashed line).

phases was developed

$$\rho_{\mathrm{Fe}} = a_0 + a_1 T + a_2 T^2 + a_3 T^3. \tag{10}$$

where $a_0 = 8.1 \times 10^3\,\mathrm{kg\,m^{-3}}$, $a_1 = -1.7 \times 10^{-1}\,\mathrm{kg\,m^{-3}\,K^{-1}}$, $a_2 = -2.6 \times 10^{-4}\,\mathrm{kg\,m^{-3}\,K^{-2}}$, and $a_3 = 2.9 \times 10^{-8}\,\mathrm{kg\,m^{-3}\,K^{-3}}$. Figure 5(a) shows a comparison of our fit with a correlation reported in the literature.

Data for the thermal conductivity of iron in the liquid[29] and solid phases[30] were fit to obtain the following expression for λ_{Fe}

$$\lambda_{\mathrm{Fe}} = b_1 T + b_2 T^2 + b_3 T^3 + b_4 T^4. \tag{11}$$

where $b_1 = 97.3\,\mathrm{W\,m^{-1}\,K^{-2}}$, $b_2 = -6.4 \times 10^{-2}\,\mathrm{W\,m^{-1}\,K^{-3}}$, $b_3 = 2.1 \times 10^{-5}\,\mathrm{W\,m^{-1}\,K^{-4}}$, and $b_4 = -2.2 \times 10^{-9}\,\mathrm{W\,m^{-1}\,K^{-5}}$. For temperatures higher than the experimental data provided in the literature, the last value of thermal conductivity has been assumed to be constant. Above 2000 K, iron is assumed to have a constant thermal conductivity of $46\,\mathrm{J\,mol^{-1}\,K^{-1}}$. Figure 5(b) shows the correlations and values reported in the literature for the given temperature ranges along with the fitted curve.

4.2 Mathematical model

The energy balance of iron and the energy balance of oxygen are described next, followed by the boundary conditions of our system. The model equations are solved in two ways, first a simplified version of the model is solved analytically to have a preliminary analysis and also to validate the numerical model, after that, the full model is solved numerically using the open-source software FEniCS.[31]

4.2.1 Iron energy balance

The iron energy balance describes how the heat is transferred along the lance, and it is mathematically described as

$$\frac{d}{dx}\left(\lambda_{\mathrm{Fe}}\frac{dT}{dx}\right) + \rho_{\mathrm{Fe}}C_{p,\mathrm{Fe}}v_{\mathrm{Fe}}\frac{dT}{dx} - S_1\sigma\epsilon_{\mathrm{Fe}}(T^4 - T_a^4) \\ -S_1h_a(T - T_a) - S_2h_{\mathrm{O_2}}(T - T_{\mathrm{O_2}}) = 0 \tag{12}$$

where T is the temperature of the iron, S_1 and S_2 are ratios of the inner diameter and outer diameter over a cross-section area, σ is the Stefan-Boltzman constant, ϵ_{Fe} is the emissivity of iron, h_a is the heat transfer coefficient from the iron to the air, $h_{\mathrm{O_2}}$ is the heat transfer coefficient from the iron to the oxygen, and $T_{\mathrm{O_2}}$ is the temperature of the oxygen. Note that the velocity of iron consumption v_{Fe} at the reaction front is dependent on the temperature at the interface and the kinetics of reaction.

The first term describes the heat conduction through the iron; the second term describes the heat convection of the solid iron receding as it is consumed; the third term describes the heat loss by thermal radiation from the lance to the air; the fourth term describes the heat loss from the lance to the air by natural convection, and the fifth term describes the forced thermal convection caused by the oxygen flowing inside the lance.

S_1 refers to the surface area in contact with the air and $\mathrm{S_2}$ refers to the surface area in contact with the oxygen. The ratios are respectively estimated by dividing the outer

perimeter in contact with the air (i.e. πd_o) and the wetted perimeter in contact with the oxygen (i.e. $\pi(d_i + nd_r)$) by the cross-sectional area $A = \pi(d_o^2 - d_i^2 + nd_r^2)/4$ of the iron in the lance.

The heat transfer coefficient due to the forced convection of oxygen is

$$h_{\mathrm{O_2}} = \frac{\mathrm{Nu}\lambda_{\mathrm{O_2}}}{D_H} \tag{13}$$

where $D_H = \frac{4\times\text{cross-sectional area}}{\text{wetted perimeter}}$ is the hydraulic diameter of the oxygen flow, and Nu is the Nusselt number calculated using the Dittus-Boelter[32] correlation

$$\mathrm{Nu} = 0.043\ \mathrm{Re}^{0.8}\mathrm{Pr}^{0.4}\left(\frac{\mu_{O_2,bulk}}{\mu_{\mathrm{O_2,wall}}}\right)^{0.14} \tag{14}$$

where $\mu_{\mathrm{O_2},bulk}$ corresponds to the oxygen viscosity at room temperature and $\mu_{\mathrm{O_2,wall}}$ is the oxygen viscosity at an estimated mean combustion temperature of 3000 K, which is 8.9×10^{-5} Pa s. The Reynolds (Re) and Prandtl (Pr) numbers are calculated as

$$\mathrm{Re} = \frac{d_i\, v_{\mathrm{O_2}}\, \rho_{\mathrm{O_2}}}{\mu_{\mathrm{O_2}}} \tag{15}$$

$$\mathrm{Pr} = \frac{C_{p,\mathrm{O_2}}\, \mu_{\mathrm{O_2}}}{\lambda_{\mathrm{O_2}}} \tag{16}$$

where $v_{\mathrm{O_2}}$ is the velocity of the oxygen flow. In the literature model,[5] the velocity of the oxygen flow is considered to be much larger than the velocity of the lance being consumed, therefore the velocity used in calculating the Reynolds number is the velocity of the oxygen flow.

The heat transfer coefficient for the natural heat convection with air is

$$h_a = \frac{\mathrm{Nu}\ \lambda_a}{\mathrm{d_o}} \tag{17}$$

where the expression used for Nu corresponds to natural convection,[32] and is calculated as

$$\mathrm{Nu} = b\left[\frac{d_o^3 \rho_a^2\, g\, \beta_a\, \Delta T}{\mu_a^2}\frac{C_{p,a}\,\mu_a}{\lambda_a}\right]^m \tag{18}$$

where $b = 1.09$ and $m = 1/5$ are constant model parameters,[5] g is the gravitational acceleration, β_a is the volume expansion coefficient of air which has a value of $0.00338\,\mathrm{K}^{-1}$ at 25°C and 1 atm, and ΔT is the temperature difference between the surface of the thermal lance, more specifically at the burning end, and the air.

To solve the differential equation for the iron energy balance, given by Eq. (12), two boundary conditions that describe each end of the thermal lance are required.

The first boundary condition is that the temperature of the rod infinitely far from the reacting tip must approach T_∞ (i.e. $T(x) \to T_\infty$ as $x \to \infty$). The second boundary condition applies at the tip of the thermic lance, which is expected to be covered by an oxide layer where the combustion of iron is expected to occur. The oxide layer is assumed to be very thin and to have a uniform temperature, equal to the tip temperature. The boundary condition at the tip (i.e. $x = 0$) is given by

$$\begin{aligned}\rho_{\mathrm{Fe}} v_{\mathrm{Fe}} \Delta H_c - \lambda_{\mathrm{Fe}}\frac{dT}{dx} \\ - h(T - T_\infty) - \sigma\epsilon_{\mathrm{FeO}}(T^4 - T_\infty^4) = 0.\end{aligned} \tag{19}$$

The first term on the left side of the equation is the rate of generation of heat due to the oxidation of iron. The second term is the conduction of heat into the iron rod. The final two terms are the heat loss to the environment from the surface of the oxide layer due to convection and radiation.

4.2.2 Oxygen energy balance

The energy balance of the oxygen accounts for the velocity of the oxygen and how it heats up due to heat convection from the lance combustion

$$\rho_{\mathrm{O}_2} C_{p,\mathrm{O}_2} v_{\mathrm{O}_2} \frac{dT_{\mathrm{O}_2}}{dx} + S_2 h_{\mathrm{O}_2}(T - T_{\mathrm{O}_2}) = 0. \tag{20}$$

The diffusion term in this case is neglected due the system being dominated by convection, where the oxygen flows due to a pressure drop, not by difference of concentrations.

The driving force for the convective heat transfer from the lance to the oxygen is the difference between the temperature of the iron and the temperature of the oxygen T_{O_2}.

4.3 Reduced model and its analytical solution

In this section, we analyze a simplified version of the thermal lance model where radiation is neglected. The reduced model still takes into account heat conduction along the lance, forced thermal convection from the lance towards the oxygen, and generation of heat from the combustion reaction. It will allow us to determine the importance of radiation. Additionally, if the parameters of the model are assumed to be constant, it can be analytically solved, which helps to validate the full model and provides a preliminary overview and better physical feel of the problem.

The energy balance equation for iron in this simplified model, which is a reduced version of Eq. (12), is given by

$$-\frac{d}{dx}\left(\lambda_{\mathrm{Fe}} \frac{dT}{dx}\right) - \rho_{\mathrm{Fe}} C_{p,\mathrm{Fe}} v_{\mathrm{Fe}} \frac{dT}{dx} + S_2 h_{\mathrm{O}_2}(T - T_{\mathrm{O}_2}) = 0. \tag{21}$$

The boundary condition of this equation at the tip of the thermal lance (cf. Eq. (19)) is

given by

$$\lambda_{\mathrm{Fe}} \frac{dT}{dx} + \Delta H_c v_{\mathrm{Fe}} \rho_{\mathrm{Fe}} = 0, \tag{22}$$

and the boundary condition as $x \to \infty$ is $T(x) \to T_\infty$. The energy balance for the oxygen is the same as Eq. (20), with an identical boundary condition.

Table 3 gives the values of the parameters of the reduced model that differ from those of the full model, which are shown in Table 2. The oxygen velocity has been estimated from Fig. 4 for an oxygen pressure over the atmospheric. The oxygen pressure has to be higher than the atmospheric pressure to reach the other end of the lance, and there is also a minimum oxygen flow required to obtain stoichiometric combustion of the iron. For the given lance dimensions, the given chemical reaction, and the given enthalpy of combustion, the minimum required oxygen flow is $1.7\,\mathrm{g\,s^{-1}}$, corresponding to an oxygen velocity of $11.6\,\mathrm{m\,s^{-1}}$.

When the parameters of the model are assumed to be constant, the solution of these two coupled linear differential equations is

$$T(z) = \frac{\Delta H_c}{C_{p,\mathrm{Fe}}} \frac{\mathrm{Pe}}{\lambda_s} e^{-\lambda_s x / L_c} + T_\infty \tag{23}$$

$$T_{\mathrm{O_2}}(x) = \frac{\Delta H_c}{C_{p,\mathrm{Fe}}} \frac{\mathrm{Bi}\,\mathrm{Pe}/\lambda_s}{\mathrm{Pe_{O_2}}\lambda_s + \mathrm{Bi}} e^{-\lambda_s x / L_c} + T_\infty. \tag{24}$$

where $\mathrm{L_c} = \frac{\text{cross-sectional area}}{\text{wetted perimeter}}$ is the characteristic length, the decay rate λ_s is given by

$$\lambda_s = \frac{1}{2}\left[\left(\mathrm{Pe} + \frac{\mathrm{Bi}}{\mathrm{Pe_{O_2}}}\right)^2 + 4\mathrm{Bi}\right]^{1/2} + \frac{1}{2}\left(\mathrm{Pe} - \frac{\mathrm{Bi}}{\mathrm{Pe_{O_2}}}\right). \tag{25}$$

with the dimensionless numbers defined as $\mathrm{Pe} = v_{\mathrm{Fe}} L_c \rho_{\mathrm{Fe}} C_{p,\mathrm{Fe}} / \lambda_{\mathrm{Fe}}$, $\mathrm{Pe_{O_2}} = v_{\mathrm{O_2}} L_c \rho_{\mathrm{O_2}} C_{p,\mathrm{O_2}} / \lambda_{\mathrm{Fe}}$, and $\mathrm{Bi} = h_{\mathrm{O_2}} L_c / \lambda_{\mathrm{Fe}}$.

According to the given lance dimensions, $\mathrm{L_c}$ is 0.7 mm. This means that the properties of the system might vary in the space of less than 1 mm, therefore if we want a numerical

Table 3: Values of the parameters used in the reduced model that are different from the full model.

Parameter	Value	Observation
ρ_{Fe} ($\mathrm{kg\,m^{-3}}$)	6980	at melting temperature
λ_{Fe} ($\mathrm{W\,m^{-1}\,K^{-1}}$)	36.3	at melting temperature
v_{Fe} ($\mathrm{cm\ s^{-1}}$)	0.8	[21]
$v_{\mathrm{O_2}}$ ($\mathrm{m\ s^{-1}}$)	15	for $P_{\mathrm{O_2}} \simeq 5$ bar
$h_{\mathrm{O_2}}$ ($\mathrm{W\,m^{-2}\,K^{-1}}$)	251.5	determined

model that captures all the changes, the mesh has to be refined accordingly.

In the reduced model, the only heat loss included is the convection from the lance to the oxygen, because it is much larger than the heat transfer from the lance to the air. To support this assumption the values of the heat transfer coefficients have been compared. The heat transfer coefficient with respect to air h_a depends on the properties of air and on the temperature of combustion. It has a value between 28 and $37\,\mathrm{W\,m^{-2}\,K^{-1}}$ for combustion temperatures between 1800 and 6000 K, respectively. The heat transfer coefficient with respect to oxygen $h_{\mathrm{O_2}}$ depends on the oxygen flow rate. It has a value between 210 and $1590\,\mathrm{W\,m^{-2}\ K^{-1}}$ for a $v_{\mathrm{O_2}}$ range between 12 and $150\,\mathrm{m\,s^{-1}}$. The heat transfer coefficient with respect to oxygen is at least 7 times larger than the heat transfer coefficient with respect to air.

The Biot number describes how the heat is transferred from the thermal lance to the surroundings. It can be calculated with respect to the oxygen $\mathrm{Bi_{O_2}}$ and with respect to the air Bi_a. Bi_a depends on the value of h_a, and it has a value between 0.004 and 0.005 for the conditions studied. $\mathrm{Bi_{O_2}}$ depends on $h_{\mathrm{O_2}}$, and it has a value between 0.004 to 0.03 for the conditions studied. For $\mathrm{Bi} \ll 0.1$, heat conduction is faster than heat convection. That means that the changes in the radial direction inside the thermal lance are very fast and the possibility of having inner temperature gradients can be neglected. This validates the choice of a one-dimensional model in which only the changes along the lance length, and not the changes in the radial direction are accounted for.

The expected heating behavior of the lance and the oxygen can be analyzed by observing

the resulting analytical expressions. The minimum temperature of the oxygen and the thermal lance is the surrounding temperature, but the temperature profile of the thermal lance increases closer to the combustion area. However, the temperature of the oxygen flowing inside the lance depends on the value of the oxygen flow rate. From the analytical solution for the temperature profiles, given in Eqs. (23) and (24), it can be observed that for $\mathrm{Pe}_{\mathrm{O}_2} \ll 1$, T_{O_2} is going to be very similar to T. This means that for low oxygen back pressures, and therefore low oxygen flow rates, the temperature of the oxygen inside the thermal lance is going to be very similar to the temperature profile of the thermal lance. If on the other hand $\mathrm{Pe}_{\mathrm{O}_2}$ is large, T_{O_2} is going to be smaller than T, meaning that for a large oxygen flow the temperature of the oxygen is going to be lower than the temperature of the thermal lance.

The dimensionless values obtained in the analytical solution for the given conditions are $\mathrm{Bi} = 0.005$ and $\mathrm{Pe} = 0.88$. The heat transfer coefficient $h_{\mathrm{O}_2} = 251.5\,\mathrm{W\,m^{-2}\,K^{-1}}$. The resulting temperature profiles can be found in Fig. 6, in this case the thermal lance reaches a temperature of 5770 K at the burning end, and the oxygen reaches a temperature of 384 K, barely increasing from its initial temperature. It should also be noted how drastically the temperature of the lance decreases in the space of 3 mm, which confirms the need of a very refined mesh when numerically solving the problem.

4.4 Comparison of the reduced problem with the numerical solution of the full problem

The full model has been solved with the finite element method (FEM) and its solution has been compared with the analytical solution of the reduced model. A further comparison has been made by using variable or constant values for the parameters ρ_{Fe} and λ_{Fe} in both, the reduced and the full model. The four cases can be calculated numerically, but the result from the reduced model with constant parameters is the same as the analytical solution already seen. The model parameters are given in Tables 2 and 3.

Figure 7 shows a comparison of the lance and the oxygen temperature profiles for the

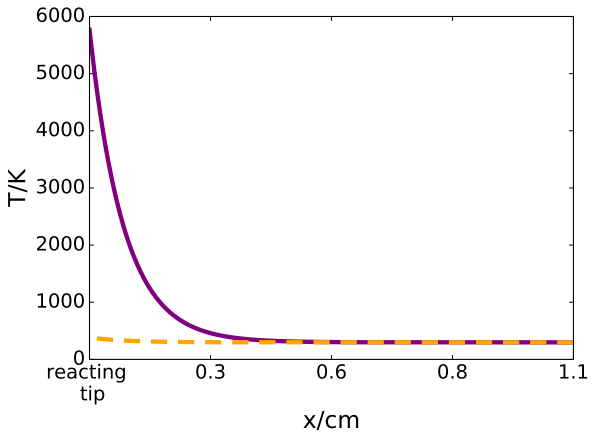

Figure 6: Analytical solution of the simplified thermal lance model with constant thermophysical parameters. Temperature profile of the thermal lance (purple solid line) and temperature profile of the oxygen (orange dashed line) along the length of the lance.

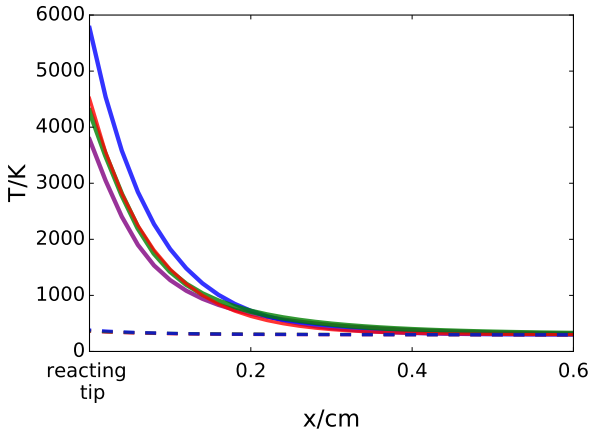

Figure 7: Comparison of the lance temperature distribution (solid line) and the oxygen temperature distribution (dashed line) from the numerical solution of different models. Reduced model and constant ρ_{Fe} and λ_{Fe} (blue), reduced model and variable ρ_{Fe} and λ_{Fe} (green), full model and constant ρ_{Fe} and λ_{Fe} (red), and full model and variable ρ_{Fe} and λ_{Fe} (purple).

four different lance models solved numerically. All the curves are very close to each other and partially overlapping, but the temperature at the burning end of the lance can be very different due to the steepness of the curve. Table 4 compares the iron and the oxygen temperature at the tip of the lance for the four models. The most complex model (4) has the lowest iron tip temperature, and the simplest model (1) has the highest iron tip tempera-

Table 4: Temperature (K) at the burning tip of the lance for the different versions of the lance model.

#	**Model**	ρ_{Fe} & λ_{Fe}	T_{tip} (lance)	T_{tip} (oxygen)
1	Reduced	constant	5770	384
2	Reduced	variable	4291	370
3	Full	constant	4516	364
4	Full	variable	3783	360

ture, meaning that the simplification mechanisms applied on the lance model contribute to increasing the tip temperature with an additive effect. It also seems that neglecting some heat transfer terms in the lance energy balance (2) has less impact than fixing the values of the model parameters (3).

4.5 Effect of latent heat

In the previous sections, we assumed that the iron rod remained in a single phase up until it undergoes the oxidation reaction at the tip. At room temperature and moderately high pressures, the stable form of iron is the solid α phase, which is a face-centered cubic crystal (ferrite). As it is heated, the solid undergoes transition at 1185 K to the γ phase (austenite), which is body-centered cubic,[33] and then another transition at 1167 K to the solid δ phase, which has face-centered cubic structure, before melting at 1811 K.[34,35] Each of these transitions is accompanied by an absorption of latent heat. The enthalpy of the α to γ transition is $900\,\mathrm{J\,mol^{-1}}$, while the γ to δ transition has an enthalpy of $8500\,\mathrm{J\,mol^{-1}}$.[34] These, however, are significantly lower than the heat of fusion, which is $13800\,\mathrm{J\,mol^{-1}}$.[34] In this section, the influence of the iron melting on the temperature profile of the thermal lance is examined. As was shown previously, in the typical operation of a thermal lance, the convection of heat from the lance to the surrounding oxygen is much slower than the conduction of heat along the lance (i.e. $\mathrm{Bi} \ll 0.1$), and so to simplify the analysis, we take the limit $\mathrm{Bi} = 0$, neglecting the convective cooling. In this case, $\lambda_s = \mathrm{Pe}$.

The layer between the solid and liquid iron can be described as a Stefan problem, involving a "moving" boundary due to a phase transition. At one side of the boundary there is a solid

phase, and at the other one a liquid phase, each of them with their own energy balance. The temperature at the interface corresponds to the melting temperature of iron of $T_m = 1811$ K. The position of the solid/liquid interface is taken to be located at $x = x_m$, and the reacting tip is at $x = 0$.

The molten and solid layers can be considered separately. Assuming that the properties of the solid and molten iron are the same, the energy balance within the molten portion of the lance, where $0 \leq x \leq x_m$, is

$$-\lambda_{\mathrm{Fe}} \frac{d^2 T_{\mathrm{liquid}}}{dx^2} - \rho_{\mathrm{Fe}} v_{\mathrm{Fe}} C_{p,\mathrm{Fe}} \frac{dT_{\mathrm{liquid}}}{dx} = 0 \tag{26}$$

where T_{liquid} refers to the molten iron. The energy balance for the solid portion of the lance, where $x \geq x_m$, is

$$-\lambda_{\mathrm{Fe}} \frac{d^2 T_{\mathrm{solid}}}{dx^2} - \rho_{\mathrm{Fe}} v_{\mathrm{Fe}} C_{p,\mathrm{Fe}} \frac{dT_{\mathrm{solid}}}{dx} = 0 \tag{27}$$

where T_{solid} refers to the solid iron.

As for the single phase analysis, we still retain the boundary conditions at $x = 0$ (see Eq. (22)), which applies to the molten layer, and at $x \to \infty$, which applies to the solid layer. However, we have two additional conditions that apply at the solid/liquid interface at $x = x_m$. The first is that the temperatures of the solid and molten phases must be equal at the interface (i.e. $T_{\mathrm{solid}}(x_m) = T_{\mathrm{liquid}}(x_m)$). The second is that the difference between the heat that conducts into the interface from the molten layer and from the interface into the solid layer is due to the heat of fusion

$$\lambda_{\mathrm{Fe}} \frac{dT_{solid}}{dx} - \lambda_{\mathrm{Fe}} \frac{dT_{liquid}}{dx} = \Delta H_m \rho_{\mathrm{Fe}} v_{\mathrm{Fe}}. \tag{28}$$

These equations can be analytically solved to give the temperature profile in the molten

portion of the lance for $0 \leq x \leq x_m$

$$T_{liquid}(z) = \frac{\Delta H_c}{C_{p,\mathrm{Fe}}} e^{-x\mathrm{Pe}/L_c} + T_\infty - \frac{\Delta H_m}{C_{p,\mathrm{Fe}}}, \tag{29}$$

and the temperature profile in the solid portion of the lance for $x_m < x$

$$T_{solid}(z) = \frac{(T_m - T_\infty)\Delta H_c}{C_{p,\mathrm{Fe}}(T_m - T_\infty) + \Delta H_m} e^{-x\mathrm{Pe}/L_c} + T_\infty. \tag{30}$$

The location x_m of the solid/liquid interface, where temperature of the lance corresponds to the melting temperature of iron, is given by

$$x_m = \frac{L_c}{\mathrm{Pe}} \ln\left(\frac{\Delta H_c}{C_{p,\mathrm{Fe}}(T_m - T_\infty) + \Delta H_m}\right). \tag{31}$$

The temperature profile of the thermal lance is shown in Fig. 8. The red curve denotes the molten portion of the lance, while the blue curve denotes the solid portion. There is a slight kink in the temperature profile at the solid/liquid interface due to the heat of fusion. This subtle change in the slope of the temperature curve before and after melting, which is not very noticeable, decreases the final tip temperature.

The tip temperature is $T_{\mathrm{tip}} = T_\infty + (\Delta H_c - \Delta H_m)/C_{p,\mathrm{Fe}}$. This should be compared to the tip temperature without the consideration of melting $T_{\mathrm{tip}} = T_\infty + \Delta H_c/C_{p,\mathrm{Fe}}$ (see Eq. (23), with $\mathrm{Bi} = 0$). These expressions for the tip temperature assume all the heat released by the iron oxidation is used to melt and heat the iron rod. The temperature at the combustion tip is 5503 K, which is lower than the tip temperature obtained in the analytical solution excluding melting but including oxygen flow of 5770 K (see Table 4). These tip temperatures are higher than the experimental adiabatic flame temperatures because of the assumptions that the heat capacity of the iron is constant and that the iron oxide remains molten. In reality, some of the molten iron oxide will decompose to iron vapor and oxygen,[36] thereby "absorbing" sensible heat and reducing the temperature.

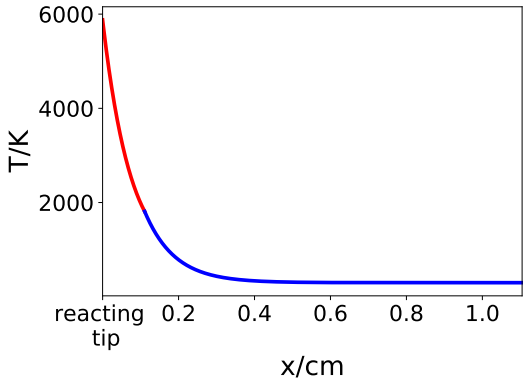

Figure 8: Temperature profile of a thermal lance including melting and excluding oxygen flow. Liquid iron (red line) and solid iron (blue line).

Up to this point a constant burning velocity was assumed, but in reality this velocity depends on the tip temperature at the reacting end. In the next section, the thermal lance model is coupled with the iron kinetics to find a tip temperature that is compatible with both, the energy balance and the reaction kinetics.

5 Consistent solutions

In this section, the thermal lance energy balance has been combined with the kinetics model in order to obtain a solution that is consistent with both. It includes the effect of the oxygen flow, but it excludes the effect of the iron melting.

As previously mentioned, the iron energy balance describes the temperature profile along the lance length, but the combustion velocity v_{Fe} that appears in the balance should be determined from combustion kinetics. Figure 9 is a scheme that shows that the iron tip temperature determines the burning velocity, and the burning velocity determines how much heat is transferred to the lance tip. At the same time, the oxygen flow rate influences the tip temperature because it takes heat away from the tip, but it also influences the burning velocity because the rate of combustion depends on the oxygen pressure. Other parameters included in the expression to determine the rate of combustion are the kinetics parameters

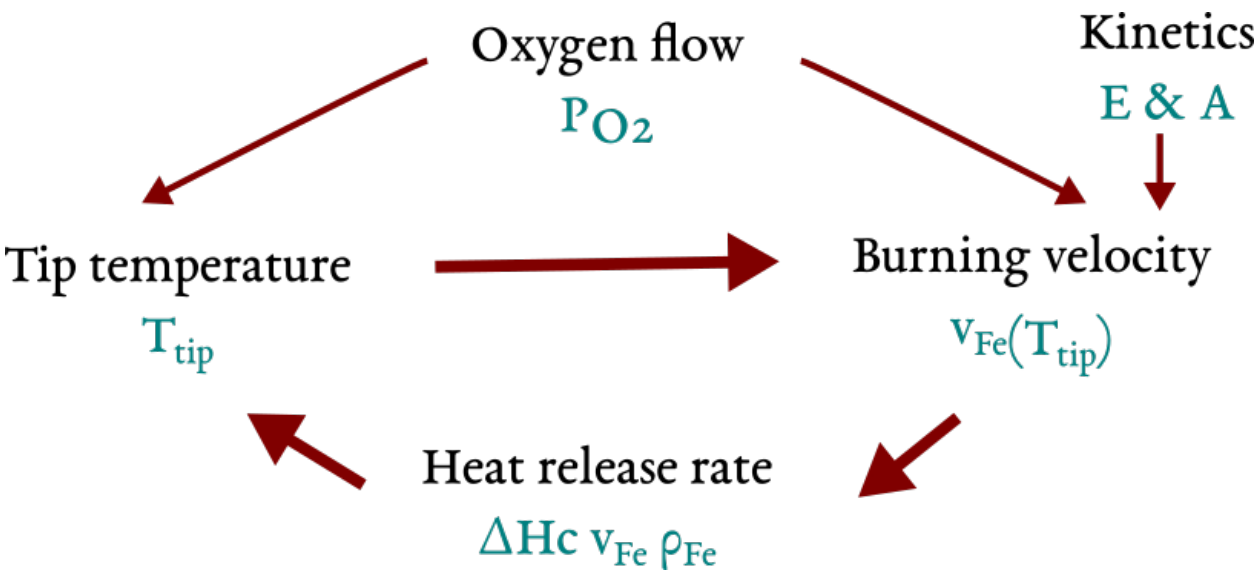

Figure 9: Dependence of the iron tip temperature on the burning velocity and other contributing factors.

characteristic of the reaction of iron oxidation.

5.1 Using the analytical solution

A prediction of the temperature profile of the lance can be obtained by using the kinetics parameters from the literature[2] to determine a burning velocity instead of using a constant value, and using an initial guess of a tip temperature. However, to make the temperature of the lance and kinetics consistent, the tip temperature predicted by the iron energy balance was used as the temperature to calculate the rate of reaction and it was assessed if the resulting rate of reaction was suitable to sustain the same temperature at the tip, which in first instance it was not.

The challenge was to find an iron tip temperature that makes the temperature profile distribution and the rate of combustion consistent with each other. To find the possible values of the tip temperature that are consistent with the energy balance and the rate of reaction, a single expression including both models has been developed.

The energy balance for the iron rods imposes a relationship between the rate of combustion, as given by v_{Fe}, and the tip temperature through the boundary condition. For the

simplified model, the analytical solution provides a relation between the rate of combustion with the tip temperature (see Eq. (23))

$$T_{\text{tip}} = \frac{\Delta H_c}{C_{p,\text{Fe}}} \frac{\text{Pe}}{\lambda_s} + T_\infty. \tag{32}$$

Neglecting the temperature change of the oxygen, the expression for λ_s can be simplified to

$$\lambda_s = \frac{\text{Pe}}{2} + \frac{1}{2}(\text{Pe}^2 + 4\text{Bi})^{\frac{1}{2}}. \tag{33}$$

The rate of reaction is directly related to the temperature at the tip by Eq. (3), which can also be written in terms of v_{Fe} as

$$R_{\text{Fe}} = A' \; e^{-E/(RT_{\text{tip}})} = \rho_{\text{Fe}} v_{\text{Fe}}. \tag{34}$$

This expression can be rearranged to give the "dependence" of the lumped pre-exponential factor on the burning rate

$$A' = \frac{\text{Pe} \; \lambda_{\text{Fe}}}{\text{L}_\text{c} \; C_{p,\text{Fe}}} \exp\left(\frac{E \; C_{p,\text{Fe}}}{\Delta H_c R \left(C_{p,\text{Fe}} T_\infty / \Delta H_c + \text{Pe}/\lambda_s \right)} \right). \tag{35}$$

Once a consistent solution is found, the value of the burning velocity can be compared with experimental data, and if the determined velocity does not match the observed velocity, then the kinetic parameters can be adjusted. The values of the kinetic parameters available in the literature may only be suitable for the specific experimental conditions in which they were determined. For that reason, it has been considered acceptable to adjust the value of the pre-exponential factor A' in order to obtain realistic burning velocities for our system. The same process of finding a consistent tip temperature is repeated for different values of the pre-exponential factor A' until a satisfactory burning velocity is found.

The sensitivity of A' to different parameters has been analyzed in Fig. 10, Fig. 11 and

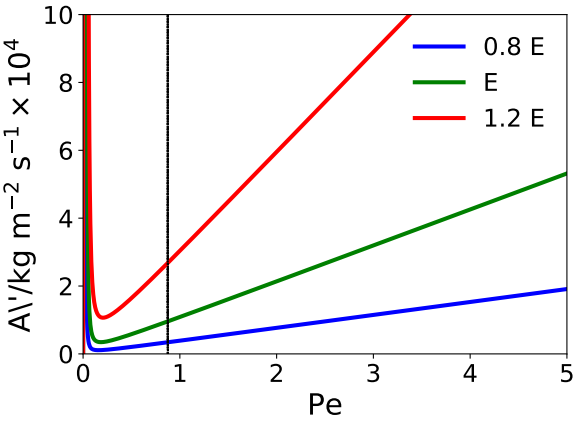

Figure 10: Sensitivity of A' to the variation of the activation energy ($E = 246.8\text{kJ mol}^{-1}$, $\Delta H_c = -253.2\,\text{kJ mol}^{-1}$, Bi $= 0.005$). Experimental Pe (dotted line).

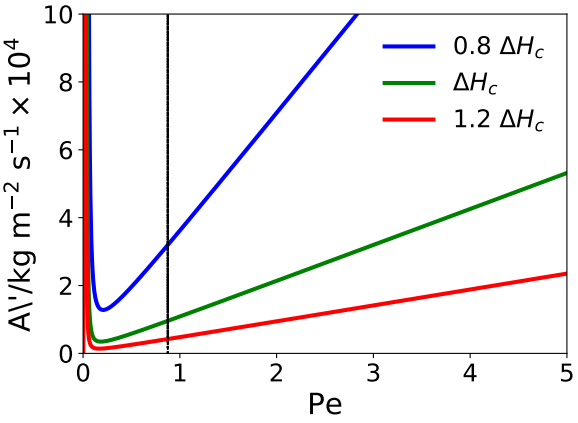

Figure 11: Sensitivity of A' to the variation of the enthalpy of reaction ($E = 246.8\,\text{kJ mol}^{-1}$, $\Delta H_c = -253.2\,\text{kJ mol}^{-1}$, Bi $= 0.005$). Experimental Pe (dotted line).

Fig. 12 by modifying the values of the activation energy, the enthalpy of reaction and the Biot number respectively. The three figures show how the value of A' changes with respect to Pe for the different values of the varying parameters, and the Peclet number determined from the experimental data has been clearly marked as a reference point.

Figure 10 shows that for the literature value of the activation energy and for the determined Peclet number, the lumped pre-exponential factor should be in the order of $9 \times 10^3\,\text{m}^{-2}\,\text{s}^{-1}$. By reducing the activation energy by a 20%, a lower A' is required, and the opposite is true when increasing the activation energy by a 20%. Figure 11 shows that in-

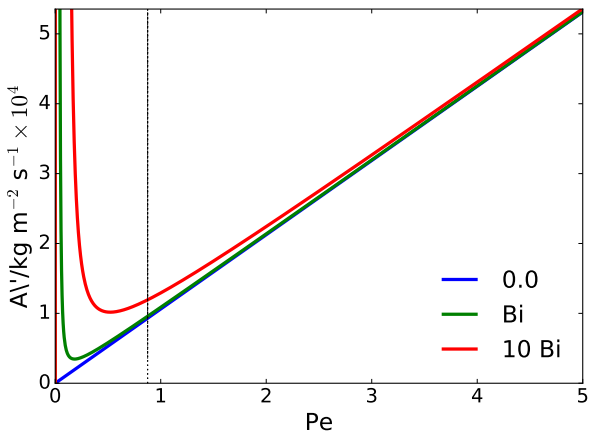

Figure 12: Sensitivity of A' to the variation of the Biot number ($E = 246.8\,\mathrm{kJ\,mol^{-1}}$, $\Delta H_c = -253.2\,\mathrm{kJ\,mol^{-1}}$, Bi $= 0.005$). Experimental Pe (dotted line).

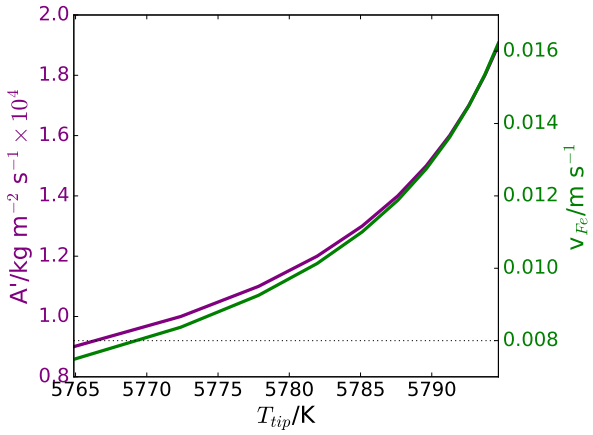

Figure 13: Iron combustion velocity and value of A' with increasing tip temperature ($E = 246.8\,\mathrm{kJ\,mol^{-1}}$, $\Delta H_c = -253.2\,\mathrm{kJ\,mol^{-1}}$, Bi $= 0.005$). Experimental combustion velocity (dotted line).

creasing the enthalpy of reaction will decrease the required A'. The magnitude of its influence is the same as that of the activation energy.

Figure 12 shows that the combustion behavior is not very much affected by having a Biot number of zero or by increasing the Bi number determined from the experimental observation by a factor of 10. Biot number is related to the heat transfer coefficient from the combustion to the oxygen, and the heat transfer coefficient is related to the velocity of the oxygen flow. From this figure it could be concluded that the velocity of the oxygen flow does not have a

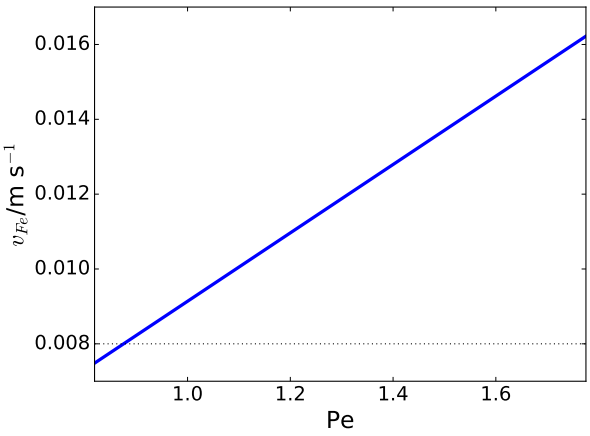

Figure 14: Iron combustion velocity with increasing Pe ($E = 246.8\,\mathrm{kJ\,mol^{-1}}$, $\Delta H_c = -253.2\,\mathrm{kJ\,mol^{-1}}$, Bi $= 0.005$). Experimental combustion velocity (dotted line).

great impact on the velocity of combustion, except for very large velocities of oxygen flow.

The relationship between A' and the velocity of combustion in relation to the temperature at the tip of the lance is shown in Fig. 13. The velocity of combustion increases with increasing tip temperature and increasing lumped pre-exponential factor. Also using the expression of Pe, Fig. 14 shows how the velocity of combustion increases with an increasing Pe.

5.2 Full numerical model

The full numerical model involves the full balance equations and variable thermal properties. In this case, on the one hand a range of given tip temperatures are used to determine the corresponding v_{Fe} for each, and on the other hand the determined v_{Fe} for each given tip temperature is used to determine a tip temperature from the iron energy balance. Finally, we see if the the given tip temperature and the determined tip temperature are the same. The velocity is calculated as follows

$$v_{\mathrm{Fe}} = \frac{A'}{\rho_{\mathrm{Fe}}} e^{-E/(RT_{tip})}. \tag{36}$$

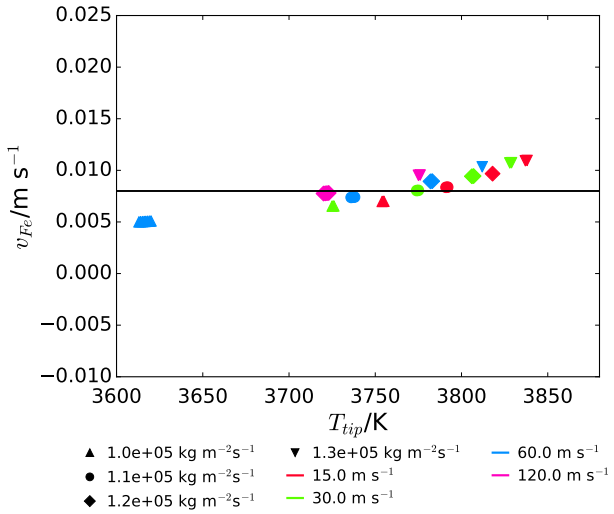

Figure 15: Combustion velocity versus tip temperature at atmospheric pressure for different pre-exponential factors (symbols) and different oxygen flows (colors). The horizontal line at $0.8\,\mathrm{cm\,s^{-1}}$ corresponds to the experimental velocity.

A consistent solution is found when the difference between the given tip temperature and the determined tip temperature from the energy balance is zero. The oxygen velocities could range from a minimum velocity of $11.6\,\mathrm{m\,s^{-1}}$ corresponding to the stoichiometric oxygen flow and assuming a burning velocity of $0.8\,\mathrm{cm\,s^{-1}}$, to a maximum oxygen velocity that is too high to sustain the iron combustion.

The velocities calculated and the given tip temperature for each case are reported in Fig. 15. For each pre-exponential factor, if a solution is not found for a given oxygen flow that appears in the legend, it means that that value is either too small or too large to give a solution.

In this case, from the experimental data, we expect a consumption velocity of approximately $0.8\,\mathrm{cm\,s^{-1}}$;[21] therefore, from all the possible consistent solutions, we would pick the conditions that match this velocity, which are a pre-exponential $1.1 \times 10^5\,\mathrm{kg\,m^{-2}\,s^{-1}}$ and an oxygen velocity of $15\,\mathrm{m\,s^{-1}}$, corresponding to an oxygen flow rate of about $2.5\,\mathrm{kg\,s^{-1}}$ and an initial back-pressure slightly above the atmospheric pressure. It should be noted that this pre-exponential factor is only an apparent kinetic parameter, not an intrinsic one, because

it lumps the effect of the oxygen absorption and the oxygen partial pressure.

The determined mean pre-exponential factor in Wilson et al.[2] transformed into the same units as the pre-exponential factor determined in this work and also for atmospheric pressure is $2.2 \times 10^4\,\mathrm{kg\,m^{-2}\,s^{-2}}$, which is smaller than the value determined in this work of $1.1 \times 10^5\,\mathrm{kg\,m^{-2}\,s^{-2}}$. This observation is not conclusive, but it seems to imply that the value determined in the literature would lead to a slower combustion velocity, and therefore that the effect of having oxygen blowing through a thermal lance would make the iron combustion faster than having an iron bar in an stagnant oxygen atmosphere.

Looking back at Fig. 2, it can be observed that for an iron rod in a stagnant atmosphere, the combustion velocity that is similar to the one observed for a thermal lance of $0.8\,\mathrm{cm\,s^{-1}}$ and for an oxygen pressure similar to the atmospheric, the iron rod in an stagnant oxygen atmosphere should be of a diameter of 0.1 cm or smaller, which according to their findings, the smaller the rod diameter, the higher is the velocity of consumption. From this observation it could be concluded that the effect of having oxygen blowing through a thermal lance is comparable at having a very thin iron rod, which seems to agree with the fact that a thermal lance is constantly blowing the molten material away and leaving the surface of the tip of the lance available to absorb more oxygen, and a smaller rod diameter has a higher surface area of molten material with respect to its volume, which increases the oxygen absorption.

6 Conclusions

This work covers a review of iron and thermal lance combustion, develops a model for the thermal lance combustion, and makes an analysis of the thermal lance operating conditions and their impact on the combustion performance.

The mathematical description for the operation of a thermal lance developed has been based on the model of Wang and co-workers[5] and on experimental data related to the combustion kinetics of iron also from the literature. A key insight from the model on the

operation of a thermal lance is that there is a "window" of possible rates at which it can burn. The location and size of this window depends on the steady-state temperature of the lance tip, which is established through interplay between the combustion reaction kinetics and the heat transfer rate.

The steady-state temperature of the lance tip is a result of the balance between the rate at which heat is generated from the combustion of the lance and the rate at which heat is transferred to its surroundings. The heat transfer rate is dependent on the properties of the surroundings, such as its temperature, thermal conductivity, relative velocity, etc. In particular, the flow rate of the oxygen supply plays a big role in dictating the heat transfer from the lance tip. It can be used to control the rate of combustion; however, it is restricted to lie within the operating window.

The operating window is delimited by a minimum and a maximum oxygen flow rate which correspond to a minimum and maximum oxygen back pressure. There is a minimum pressure required for the oxygen to reach the other side of the thermal lance, and there is also a minimum amount of oxygen required for stoichiometric combustion of the total mass of iron. The maximum oxygen pressure is reached when the oxygen flow takes too much heat away from the combustion zone, decreasing its temperature. Below the minimum oxygen back pressure the combustion will not happen. Above the maximum oxygen back pressure the combustion could still happen, but it would not be self-sustained and it would require an external source of heat. The minimum oxygen pressure to reach the other end of the lance can be determined independently of the combustion reaction rate, but the minimum stoichiometric oxygen required and the maximum oxygen flow, both depend on the combustion reaction rate.

The suggested kinetics parameters found for a thermal lance at atmospheric pressure are an activation energy of $246.8\,\mathrm{kJ\,mol^{-1}}$, a pre-exponential factor of $1.1 \times 10^5\,\mathrm{kg\,m^{-2}s^{-1}}$, and an oxygen back pressure slightly over the atmospheric pressure. These parameters could be further adjusted given additional experimental data.

Nomenclature

Latin symbols

ΔH	Enthalpy
$\dot{m}$	Mass flow rate
A	Iron cross-sectional area
A	Pre-exponential factor
A'	Apparent pre-factor
C_p	Heat capacity
D_H	Hydraulic diameter
d_i	Inner tube diameter
d_o	Outer tube diameter
d_r	Rod diameter
E	Activation Energy
f	Friction factor
h	Heat transfer coefficient
K	Adsorption equilibrium constant
k	Rate constant
k'	Apparent rate constant
n	Number of rods
p	Pressure

P_{O_2} Oxygen partial pressure

P_{wet} Inner wetted perimeter

R Gas constant

R_{Fe} Rate of reaction

S_1 Normalized surface area in contact with air

S_2 Normalized surface area in contact with oxygen

T Temperature

v_{Fe} Velocity of iron cosumption

v_{O_2} Oxygen velocity

x Distance along the lance from the reacting tip

y Distance along the lance from the oxygen injection

Bi Biot number

Nu Nusselt number

Pe Peclet number

Pr Prandtl number

Re Reynolds number

Subscripts

∞ Surrounding environment

a Air

c Combustion

m Melting

Fe Iron

FeO Iron(II) oxide, wüstite

O_2 Oxygen

Greek symbols

β Volume expansion coefficient

ϵ Emissivity constant

λ Thermal conductivity

λ_s decay rate of temperature profile

μ Dynamic viscosity

ρ Density

σ Stefan-Boltzman constant

References

(1) U.S. Navy, Underwater cutting & welding manual. SO300-BB-MAN-010: 910-LP-111-3300, Published by direction of Commander, Naval Sea Systems Command, 1989.

(2) Wilson, D.; Steinberg, T.; Stoltzfus, J. Thermodynamics and kinetics of burning iron. *ASTM Spec. Tech. Publ.* **1997**, *1319*, 240–257.

(3) Shabunja, S. I.; Martynenko, V. V.; Ignatenko, V. I. Simulation of iron rods combustion in oxygen with the drop detachment. *Energetika* **2013**, *59*, 105–112.

(4) Benjamin Lynn, D.; Steinberg, T.; Sparks, K.; M. Stoltzfus, J. Defining the Flammability of Cylindrical Metal Rods Through Characterization of the Thermal Effects of the Ignition Promoter. *Journal of ASTM International* **2009**, *6*, 1–12.

(5) Wang, H.; Hlavacek, V.; Pranda, P. Model Analysis of Thermal Lance Combustion. *Ind. Eng. Chem. Res.* **2004**, *43*, 4703–4708.

(6) Steinberg, T. A.; Mulholland, G. P.; Wilson, D.; Benz, F. J. The combustion of iron in high-pressure oxygen. *Combust. Flame* **1992**, *89*, 221 – 228.

(7) Steinberg, T. A.; Wilson, D. B. In *Flammability and sensitivity of materials in oxygen-enriched atmospheres*; Steinberg, T., Newton, B., Beeson, H., Eds.; ASTM International: West Conshohocken, PA, 2000; Vol. 9; pp 226 – 289.

(8) Steinberg, T. A.; Kurtz, J.; Wilson, D. B. The Solubility of Oxygen in Liquid Iron Oxide During the Combustion of Iron Rods in High-Pressure Oxygen. *Combust. Flame* **1998**, *113*, 27–37.

(9) Sato, J.; Sato, K.; Hirano, T. Fire spread mechanisms along steel cylinders in high pressure oxygen. *Combust. Flame* **1983**, *51*, 279–287.

(10) Sato, J. In *Flammability and sensitivity of materials in oxygen-enriched atmospheres*; Steinberg, T., Newton, B., Beeson, H., Eds.; ASTM International: West Conshohocken, PA, 1989; Vol. 4; p 162–177.

(11) Suvorovs, T. Promoted ignition testing : An investigation of sample geometry and data analysis techniques. Ph.D. thesis, Queensland University of Technology, 2007.

(12) Hirano, T.; Sato, K.; Sato, Y.; Sato, J. Prediction of Metal Fire Spread in High Pressure Oxygen. *Combust. Sci. Technol.* **1983**, *32*, 137–159.

(13) Wright, A.; Goroshin, S.; Higgins, A. Combustion time and ignition temperature of

iron particles in different oxidizing environments. 25th ICDERS, Leeds, UK. August 2-7, 2015.

(14) Cashdollar, K. L.; Zlochower, I. A. Explosion temperatures and pressures of metals and other elemental dust clouds. *J. Loss Prev. Process Ind.* **2007**, *20*, 337 – 348.

(15) Abbud-Madrid, A.; Fiechtner, G.; Branch, M.; Daily, J. Ignition and combustion characteristics of pure bulk metals: Normal-gravity test results. 32nd Aerospace Sciences Meeting and Exhibit, American Institute of Aeronautics and Astronautics, Reno, NV, USA. January 10-13, 1994.

(16) General operating procedures for burning bars and lance pipe. Minco Pipe Inc.: Texas, USA, https://strykersteeltube.com/wp-content/uploads/2014/01/General-Operating-Procedures-for-Burning-Bars-and-Lance-Pipe.pdf.

(17) Thermic lance user guide. Tube Special: Dunaharaszti, Hungary, http://tube-special.com/wp-content/uploads/2013/02/THERMIC-LANCE-USER-GUIDE_TS.pdf.

(18) Thermic lance manual. Daiwa Lance International Co. Ltd., 2014; http://engefund.emdesenvolvimento.net/wp-content/uploads/sites/781/2017/05/Thermic-Lance-Manual.pdf.

(19) Information about the oxygen thermic lance. W. Humberg GmbH & Co. KG: Wetter, Germany.

(20) Broco Operating instructions manual for PRIME-CUT ultrathermic cutting system. Broco, Inc.: Ontario, CA 91761, USA.

(21) Clearwell Technology Limited, 2019; Private communications.

(22) Denn, M. M. *Process Fluid Mechanics*; Prentice-Hall International Series: Hoboken, NJ, USA, 1979.

(23) Laurendeau, N. M.; Glassman, I. Ignition Temperatures of Metals in Oxygen Atmospheres. *Combust. Sci. Technol.* **1971**, *3*, 77–82.

(24) Bolobov, V. Conditions for Ignition of Iron and Carbon Steel in Oxygen. *Combustion Explosion and Shock Waves* **2001**, *37*, 292–296.

(25) Chase, M. W. *NIST-JANAF Thermochemical Tables*, 4th ed.; American Institution of Physics, 1998.

(26) Assael, M. J.; Kakosimos, K.; Banish, R. M.; Brillo, J.; Egry, I.; Brooks, R.; Quested, P. N.; Mills, K. C.; Nagashima, A.; Sato, Y.; Wakeham, W. A. Reference Data for the Density and Viscosity of Liquid Aluminum and Liquid Iron. *J. Phys. Chem. Ref. Data* **2006**, *35*, 285–300.

(27) Grosse, A.; Kirshenbaum, A. The densities of liquid iron and nickel and an estimate of their critical temperature. *J. Inorg. Nucl. Chem.* **1963**, *25*, 331 – 334.

(28) Watanabe, S.; Tsu, Y.; Takano, K.; Shiraishi, Y. Density of Pure Iron in Solid and Liquid States. *J. Jpn. Inst. Met.* **1981**, *45*, 242–249.

(29) Assael, M.; Chatzimichailidis, A.; Antoniadis, K.; Wakeham, W.; Huber, M.; Fukuyama, H. Reference correlations for the thermal conductivity of liquid copper, gallium, indium, iron, lead, nickel and tin. *High Temp. High Press.* **2017**, *46*, 391–416.

(30) Powell, R. W.; Ho, C. Y.; Liley, P. E. Thermal conductivity of selected materials. Report NSRDS-NBS1966. NSRDS-NBS 8 National Standard Reference Data Series- National Bureau of Standards—8.Prepared under contract at the Thermophysical Properties Research Center Purdue University, West Lafayett, IN 47906, USA, 1966.

(31) Alnæs, M. S.; Blechta, J.; Hake, J.; Johansson, A.; Kehlet, B.; Logg, A.; Richardson, C.; Ring, J.; Rognes, M. E.; Wells, G. N. The FEniCS Project Version 1.5. *Archive of Numerical Software* **2015**, *3*, 9–23.

(32) Green, D. W., Perry, R. H., Maloney, J. O., Eds. *Perry's Chemical Engineers' Handbook*, 7th ed.; McGraw-Hill: New York, 1999.

(33) Magomedov, M. N. Changes in the Properties of Iron during BCC–FCC Phase Transition. *Phys. Solid State* **2021**, *63*, 215–222.

(34) Desai, P. D. Thermodynamic Properties of Iron and Silicon. *J. Phys. Chem. Ref. Data* **1986**, *15*, 967–983.

(35) Dorogokupets, P. I.; Dymshits, A. M.; Litasov, K. D.; Sokolova, T. S. Thermodynamics and Equations of State of Iron to 350 GPa and 6000 K. *Sci. Rep.* **2017**, 41863.

(36) Steinberg, T. A.; Wilson, D. B.; Benz, F. The combustion phase of burning metals. *Combust. Flame* **1992**, *91*, 200–208.

Graphical TOC Entry